

A new flow co-culture system for studying mechanobiology effects of pulse flow waves

Devon Scott-Drechsel · Zhenbi Su ·
Kendall Hunter · Min Li · Robin Shandas ·
Wei Tan

Received: 2 August 2011 / Accepted: 21 February 2012 / Published online: 18 April 2012
© Springer Science+Business Media B.V. 2012

Abstract Artery stiffening is known as an important pathological change that precedes small vessel dysfunction, but underlying cellular mechanisms are still elusive. This paper reports the development of a flow co-culture system that imposes a range of arterial-like pulse flow waves, with similar mean flow rate but varied pulsatility controlled by upstream stiffness, onto a 3-D endothelial-smooth muscle cell co-culture. Computational fluid dynamics results identified a uniform flow area critical for cell mechanobiology studies. For validation, experimentally measured flow profiles were compared to computationally simulated flow profiles, which revealed percentage difference in the maximum flow to be <10, <5, or <1% for a high, medium, or low pulse flow wave, respectively. This comparison indicated that the computational model

accurately demonstrated experimental conditions. The results from endothelial expression of proinflammatory genes and from determination of proliferating smooth muscle cell percentage both showed that cell activities did not vary within the identified uniform flow region, but were upregulated by high pulse flow compared to steady flow. The flow system developed and characterized here provides an important tool to enhance the understanding of vascular cell remodeling under flow environments regulated by stiffening.

Keywords Arterial stiffening · Co-culture · Flow culture chamber · Flow pulsatility · Shear stress

Introduction

Arterial stiffening is increasingly recognized as an important factor involved in cardiovascular events. Studies have suggested that stiffening of large elastic arteries influences the progression of vascular diseases and/or the aggravation of small artery remodeling in vital organs such as kidney and brain (McVeigh et al. 1999; Weber et al. 2004; Safar and Lacolley 2007; Cheung et al. 2007; Mitchell 2008; O'Rourke and Safar 2005), but the underlying mechanisms remain elusive.

Large arteries, due to their high compliance, constitute a hydraulic buffer that converts high pulse flow into continuous semi-steady flow, thereby dissipating the hemodynamic energy of high pulse flow

Electronic supplementary material The online version of this article (doi:10.1007/s10616-012-9445-2) contains supplementary material, which is available to authorized users.

D. Scott-Drechsel · Z. Su · R. Shandas · W. Tan (✉)
Department of Mechanical Engineering, University
of Colorado at Boulder, Boulder, CO 80309, USA
e-mail: wei.tan-1@colorado.edu

K. Hunter · M. Li · R. Shandas · W. Tan
Department of Bioengineering, University of Colorado
at Denver, Aurora, CO 80045, USA

K. Hunter · M. Li · R. Shandas · W. Tan
Department of Pediatrics-Cardiology, University
of Colorado at Denver, Aurora, CO 80045, USA

ejected by the heart (Safar et al. 2003; McVeigh et al. 1999). This, referred as “windkessel” effect, diminishes when the wall of large arteries hardens due to hypertension, aging or diabetes. Decrease in large artery distensibility thus let high pulse flow extend to downstream arteries (Mitchell 2008). Increased pulse flow, a direct consequence of arterial stiffening, has been used to guide pharmaceutical treatment for a variety of vascular diseases (Safar and Lacolley 2007; Weber et al. 2004). Recently, this stiffening-related effect has also been demonstrated in the pulmonary circulation (Hunter et al. 2008; Chesler et al. 2004; Gorgulu et al. 2003; Berger et al. 2002); increased pulmonary artery (PA) stiffness was correlated to clinical outcome of PA hypertension. However, PA hypertension as well as some other vascular diseases is traditionally characterized by endothelial dysfunction and smooth muscle thickening in small arteries (Sakao et al. 2009). Based on these observations, questions arise regarding the mechanistic relationship between stiffness of upstream large artery and dysfunction of small artery cells; addressing this relationship may lead to novel therapeutic targets. To explore this novel mechanistic relationship, a new flow system that mimics flow dynamics and vascular wall remodeling is in need. Currently, no *in vitro* cell culture systems allow one to study effects of artery stiffness in the macrocirculation on cell dysfunction in the microcirculation.

The present study developed a new flow co-culture system, in which influences of upstream stiffness on downstream small artery cells was achieved through dynamics of PA-like pulse flow waves that induce cell responses. The developed system presented here adopts a stiffness-adjustment chamber and a 3-dimensional (3D) tissue-mimetic co-culture chamber. Computational study was used as a design tool to describe the wave propagation and the spatial variation of the pulse flows in the co-culture chamber. The flow system was then uniquely validated with cell analyses.

Methods

Flow system setup

The flow system and the design of flow units are illustrated in Fig. 1. The system includes a blood pump, an upstream stiffness-adjustment chamber, a flow meter which exists only during the system setup, a

downstream flow co-culture chamber and a medium reservoir (Fig. 1a). A physiological pulse flow wave is created by a blood pump (Harvard Apparatus, Plymouth/PA, USA) whose flow output simulates the ventricular pumping of the heart. This pump is often used to circulate blood flow in living animals simulating the actions of the heart for perfusion. It generates the systolic and diastolic phases of pulse flow and allows for frequency adjustment. In this study, 60 beats per min is used as the beating pulse frequency of the blood pump. The tissue-mimetic 3D co-culture flow chamber is a modified parallel plate flow chamber (Fig. 1b). The detailed description is given in Sect. “Flow co-culture of smooth muscle cells and endothelial cells”. The flow is imposed onto endothelial cells (EC) co-cultured with smooth muscle cells (SMC). The test region of the chamber is 30 mm in width and 60 mm in length. The top plate of the flow chamber is made from acrylic and is held to a glass slide through vacuum channel which is carved groove circuit around the periphery of the chamber with two ports connected to the house vacuum. The vacuum is applied to hold the parallel plate flow chamber and 3D cell co-culture together preventing fluid leakage. Fluid enters the chamber through a fluid inlet port and expands into the inlet manifold before entering the cell seeded flow region. The inlet manifold allows the flow to be evenly distributed across the width of the cell-seeded area before it propagates along the chamber length.

The stiffness-adjustment chamber is custom designed and featured with an air release valve that allows one to adjust pulse flow (Fig. 1c). It is used to vary the pulsatility or pulse amplitude of the flow wave from the blood pump without changing the mean flow rate. As the total volume of the air and liquid is constant, the level of liquid in the chamber under the static condition is an indicator to the level of flow pulsatility. The cylinder of this chamber was graduated to reflect the liquid/air ratio which is correlated with the pulsatility of the resultant flow waveform. The air release valve is open to begin the experiment allowing the entrance of fluid until the level of liquid reached a predetermined level based on the desired outlet flow pulsatility. Closure of the air release valve sets the liquid/air ratio and maintains the desired flow pulsatility. As air is compressible and the medium (liquid) is not, air stores the systolic (peak) pressure energy and dampens the pulse pressure of the flow wave. Therefore, decreasing the liquid/air ratio allows

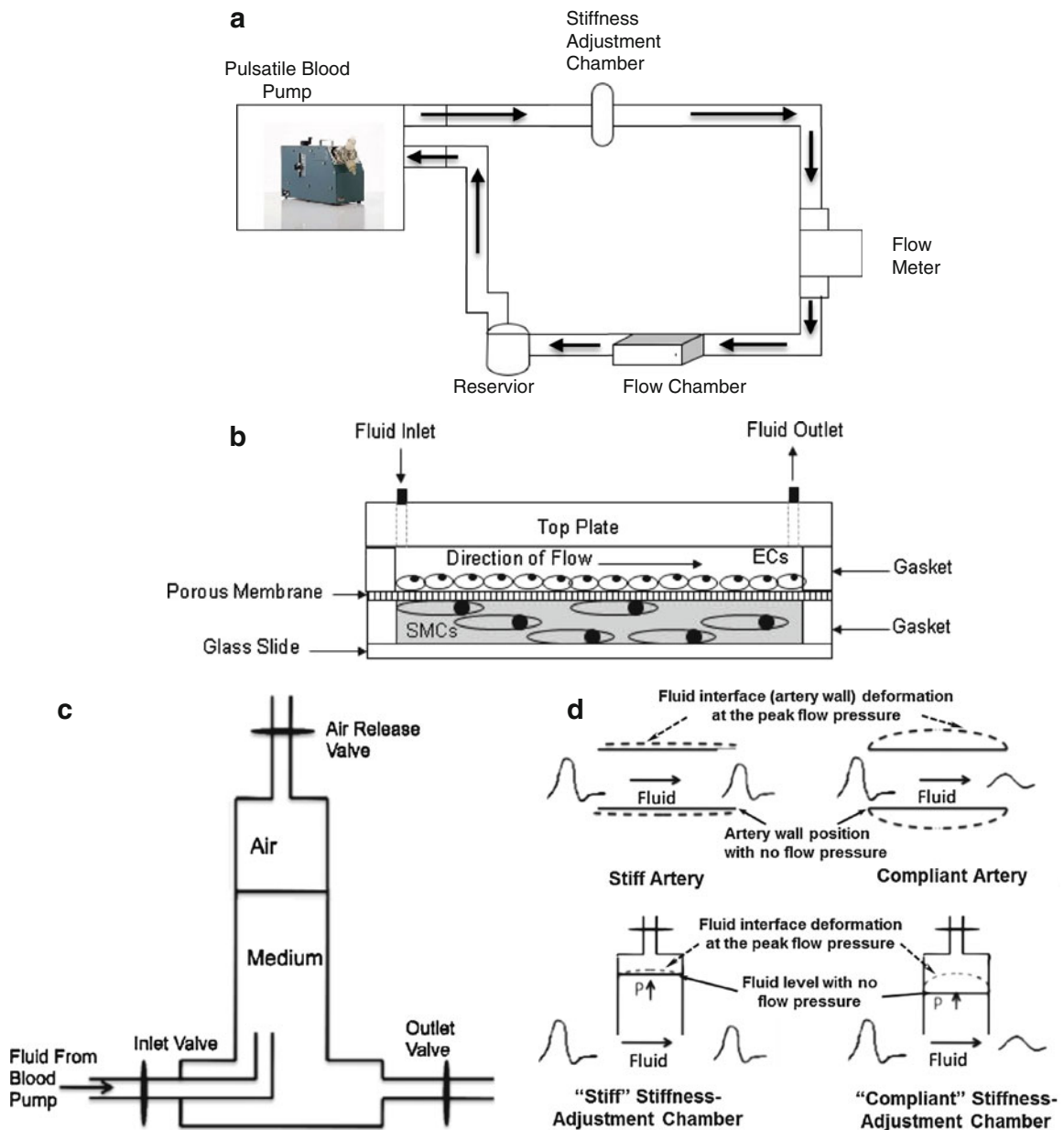


Fig. 1 Schematic illustrations of the flow system (a), the mimetic co-culture chamber (b), the stiffness-adjustment chamber (c), and function similarity between a stiffness-adjustment chamber and an upstream large artery (d). **a** The flow system demonstrates the flow circulation through different flow units. The *arrows* show the flow direction. **b** Illustration shows the cross-sectional view of a flow coculture chamber with EC seeded on a porous membrane in contact with SMCs embedded in a 3D collagen matrix. **c** The stiffness-adjustment chamber has an air release valve for adjustments of liquid/air ratio as well as inlet and outlet valves allowing medium to flow through the chamber. Air in the chamber can absorb high pulse energy and reduce pulsatility of the flow wave. **d** An illustration

shows how the stiffness-adjustment chamber simulates the elastic function of the upstream elastic artery. The chamber is a representative of the upstream artery in terms of its flow modulation function. A “stiff” chamber containing little air represents a stiff artery, which can barely expand at peak flow pressure resulting in an unmodified high pulse flow wave at the exit of the chamber. A “compliant” chamber characterized by a high air-to-liquid ratio represents a normal elastic artery, which is capable of undergoing large expansion under the peak (systolic) flow pressure, thus resulting in a dampened flow. The interface expansion shows moving of the fluid position in the flow chamber or the artery wall under the peak (systolic) flow pressure

the chamber to store more pulse pressure energy, increasing the “compliance” or damping capability of the chamber and resulting in a decrease in pulse amplitude or flow pulsatility. No membranes exist between air and medium in the chamber; the volume of compressible air is used to control the compliance.

As illustrated in Fig. 1d, the stiffness-adjustment chamber simulates the compliance function of large artery and serves to modulate the pulse flow waveform for downstream cell culture. Downstream artery cells experience flow conditions modulated by the upstream vessel. Similar to a compliant artery whose distensible wall expands to dampen systolic pressure, the stiffness-adjustment chamber with a low liquid/air ratio can function as a “compliant chamber” in which the liquid-air interface is deformable. Through the interface deformation, the medium volume in the chamber increases during the systolic phase. The fluid leaving the compliant chamber or artery thus exhibits low pulsatility. Because the excess flow is temporarily stored in the deformed interface of the chamber, the pulse flow waves vary without changing the mean flow rate much like the function of a large artery. Similarly, a “stiff” chamber containing little air simulates mechanical function of a stiff artery. Both have rigid interfaces that constrict the fluid volume, and thus are not responsive to the pressure or flow variations. Therefore, the flow leaving a “stiff” chamber or artery shows high pulsatility.

Figure 2 illustrates three flow waveforms created by adjustments of upstream stiffness. Quantitative description of the flow waveforms is detailed in Sect. “Quantification of flow waveform”. The flow system enables the individual components of flow, i.e. the mean flow magnitude, flow pulsatility and frequency, to be separately controlled and investigated.

Experimental measurements

Real-time flow rate was determined with a precision flow meter (Alicat Scientific, Tucson/AZ, USA) connected to an oscilloscope (Agilent Technologies, Santa Clara, CA) and a computer; pressure was determined with a digital pressure gauge (Colepalmer, Vernon Hills/IL, USA). To obtain the experimental input and output flow waveforms, the digital flow meter was placed either at the entrance or the exit of the culture chamber. This allowed one to visualize the

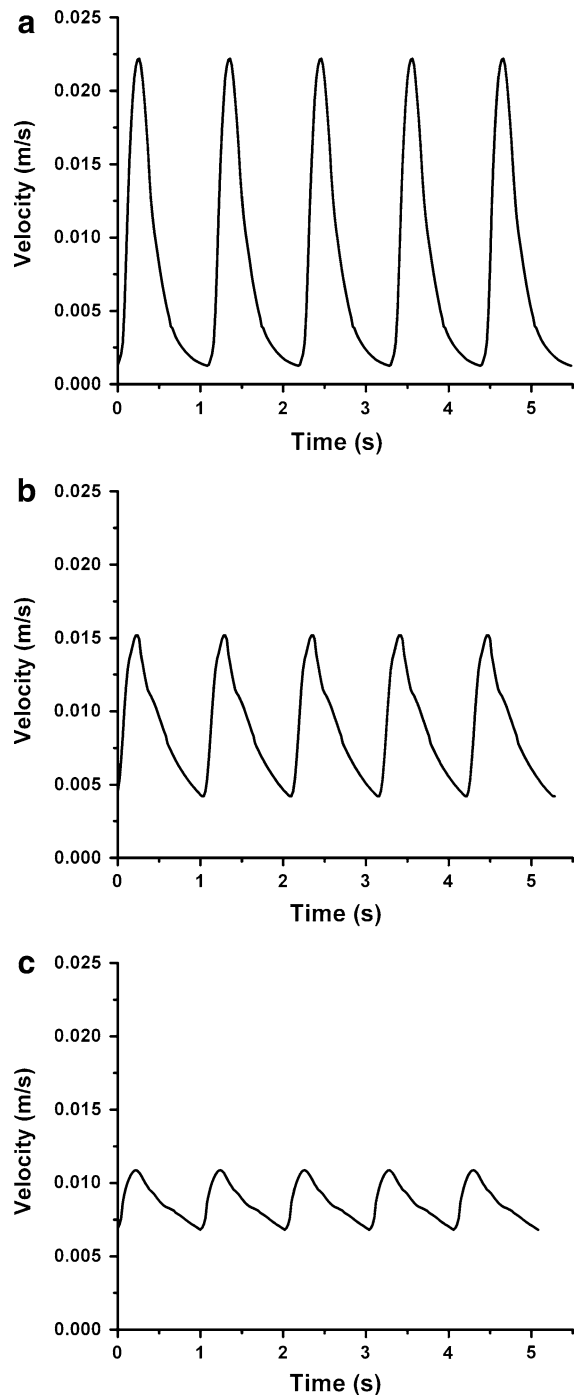


Fig. 2 The three inlet velocity time history profiles used in this study. Each *graph* displays a different velocity profile for high (a), medium (b), and low (c) pulsatility

flow wave and to quantitatively determine the mean flow rate and dynamic flow rates at specific time points.

Computational methods

Computational fluid dynamics (CFD) modeling was used as a design tool for identifying a uniform flow region. It provided maps of velocity, flow and shear stress at locations throughout the flow chamber. As CFD results were highly dependent on boundary and initial conditions, these conditions closely matched experimental measures. The validation of computational results was performed by comparing CFD results at outlet with actual measures for a sub-set of flow conditions.

First, a 3-dimensional (3-D) CFD model was created. The computational model included the entrance, a manifold and the flow culture region. Because of symmetric geometry, it is tenable to assume that the spatially non-uniform flows at the inlet and exit are approximately equal in size. A rectangular mesh was employed in the computation domain with grid spacing of 13 μm (Fig. 3). The grid spacing was determined with a grid convergence or sensitivity study that terminated upon finding changes of less than 1% in velocities between refinements at five selected locations in the model (Table 1). The geometry and grid structure were both generated with CFD-GEOM (ESI Group, Paris, France).

Due to the unique flow distribution along the length of the chamber, a two dimensional (2-D) rigid model was developed to simplify the 3-D rigid model. As the experimental setup included a membrane and collagen surface (Fig. 1b), a 2-D model with fluid structure interaction (FSI) was further developed based on the

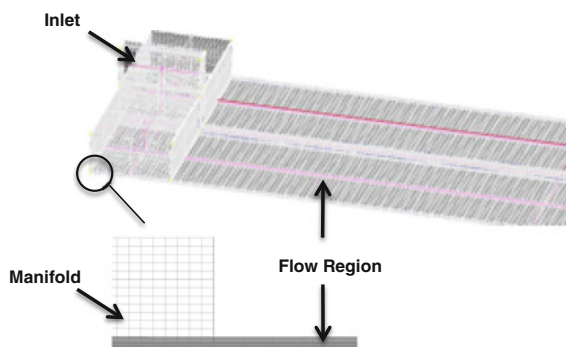


Fig. 3 The computational grid for the 3-D rigid flow chamber. The grid is refined until there is less than a 1% difference in the velocity values. Half the chamber is modeled including the inlet where fluid enters the chamber, and the manifold where fluid expands across the width of the chamber

rigid 2-D model. The solid portion of the model represented the membrane surface. The thickness of fluid and membrane was 0.5 mm.

The fluid in the models, cell medium, was modeled as an incompressible, Newtonian fluid with viscosity of 0.703 mPa·s and density of 933 kg/m³. The stress tensor was continuous across the fluid structure boundary, where the no-slip condition was applied to the fluid velocity tensor. The inlet flow rate was transient; the pulse flow waves were obtained from experimental measurements (Fig. 2). The outlet boundary condition of the flow domain was specified as a resistance boundary condition which related pressure to flow, $R = P/Q$, in which R was the resistance, P and Q were the mean pressure and flow rate from the experimental data.

The solid portion in the 2-D FSI model, which represented the deformable substrate in the experimental setup (Fig. 1b), was considered as an incompressible isotropic linear elastic material with density of 3,100 kg/m³ and Poisson's ratio of 0.5, taken from the properties of the porous membrane. The sidewalls were constrained while the exterior boundary surface had zero displacement due to an attached glass slide (in the experimental setup), and the interior boundary surface was loaded with fluid pressure/shear stress. The CFD-ACE multiphysics package (CFD Research Corporation, CA, USA) was used to develop the numerical model, to generate mesh, and to solve the governing equations for fluid flow and equations for structure mechanics. The governing equations for flow dynamics are the equations for momentum and mass conservation:

Table 1 Grid validation for the computational model

Nodes	Velocity (m/s)	Percent difference
10,200	0.0255	
19,380	0.0342	34.4
31,440	0.0242	29.4
73,745	0.0258	6.92
102,000	0.0261	1.2
157,100	0.0258	1.4
2,480,000	0.0256	0.78

Refined grids were compared with the velocity at a time of 0.7 s in the middle of the channel. The model was refined until there was a percentage difference of less than 1%

$$\rho \left(\frac{\partial \mathbf{v}}{\partial t} + \mathbf{v} \cdot \nabla \mathbf{v} \right) = -\nabla p + \mu \nabla^2 \mathbf{v} + \mathbf{f}$$

$$\nabla \cdot \mathbf{v} = 0$$

where ρ is the fluid density, \mathbf{v} is the velocity, p is the pressure, μ is the viscosity and \mathbf{f} is the body forces on the fluid. The governing equation for the structure mechanics is:

$$\rho^s \left(\frac{\partial^2 \mathbf{y}}{\partial t^2} - \mathbf{f}^s \right) = \nabla \cdot \boldsymbol{\sigma}^s$$

where \mathbf{y} is the structure displacement, the superscript s represents the properties for the structure and $\boldsymbol{\sigma}^s$ is the Cauchy stress tensor. A rectangular mesh was generated for the 2-D FSI model; the total mesh number was 3003 in fluid domain and 606 in solid domain. The time step was 5 ms and a total time of 3 s was calculated for all the cases to ensure that the simulations were convergent.

The CFD-ACE multiphysics package was used to solve the model. Briefly, this package used the finite volume method for spatial discretization of the Navier-Stokes equations and the SIMPLEC method for the continuity equation. A first-order upwind velocity rule was chosen to discretize the convective terms, and the algebraic multi-grid method was chosen to solve the resulting matrix equations. After each spatial grid convergence, a second order Crank-Nicolson algorithm was used to advance the solution in time. The CFD model used boundary and initial conditions that closely matched experimental conditions. Experimentally measured inlet flow profiles, taken at the exit of the stiffness-chamber, were used as a transient inlet boundary condition for the computational model.

Analysis of flow profile in the culture chamber

To determine if the flow in the culture channel was laminar, Reynolds number (Re) was calculated; the peak Re value for low, medium and high pulse flows were 22.2, 24.2, and 29.8, respectively. Therefore, there were laminar flows in all the flow conditions.

To examine the flow propagation, flow data from the computational solution was analyzed at different longitudinal points along the culture chamber. These points were taken from the bottom layer of fluid (the layer that directly affects the cells) at the inlet, middle and outlet of the flow region. To obtain the entrance

length, velocity values were taken at one time point longitudinally from the exit of the manifold or the beginning of the test region until the velocity variation was less than 1%. To understand spatial variation of flow velocity, velocity values were obtained horizontally across the 3-D chamber from one wall to the opposite wall, thus yielding a velocity profile across the width of the chamber. Spatial variation was also mapped over the flow region depth, measuring at one time point from the bottom up through the top layer of fluid. The shear stress was calculated from the fluid velocity with the standard expression: $\tau = \mu(\partial u/\partial y)$, where μ was the dynamic viscosity and $\partial u/\partial y$ was the spatial gradient of the chamber primary velocity normal to the chamber wall.

To determine whether pulse flow waves follow a normal parabolic profile as the flow proceeds down the chamber, the Womersley number was calculated. The degree of departure from parabolic flow increases with the Womersley number. This number is given for a rectangular chamber by the equation: $\alpha = h\sqrt{\pi/\nu}$ (Hsiai et al. 2002), where h is the height of the channel, π is $2\pi f$ and related to the flow frequency, and ν is the kinematic viscosity. The number is calculated for each flow condition.

Quantification of flow waveform

To quantify the level of flow pulsatility of the pulse flow waves, the following parametric approaches were taken: (a) calculation of the pulsatility index (PI) (b) evaluation of spectral content using a discrete fast Fourier transform (DFT), and (c) calculation of the hemodynamic energy. The PI of flow is commonly used in the evaluation of vascular stiffening effects and the evaluation of vascular diseases (Panaritis et al. 2005). It is defined as: $PI = (V_{max} - V_{min})/V_{mean}$, where V_{max} is the peak systolic velocity, V_{min} is the minimum forward diastolic velocity and V_{mean} is the average velocity. Our results showed that the PI values for the high, medium, and low pulse flow waves were 2.67, 1.68, and 0.775, respectively. Spectral analysis with DFT was performed with MATLAB software (Matworks, Natick/MA, USA) yielding the modulus based on harmonics allowing the flow wave to be decomposed into a constant mean flow and a series of sine waves or harmonics. The Fourier transform is a mathematical operation that decomposes a signal into

its constituent frequencies. The original signal (i.e. flow wave) depends on time, whereas the Fourier transform depends on frequency and is called the frequency domain representation of the signal. As cells are sensitive to the frequency of the flow wave, the harmonic frequency of each of the flow waves is compared to correlate frequency-based waveform analysis with cell behavior. The frequency of the first harmonic is the fundamental frequency and used as a measure of flow pulsatility. The first and second harmonic was analyzed to examine differences in frequency content among the three flow waveforms used in this study (Fig. 4). The high pulse flow showed the highest moduli at both harmonics, followed by the medium and finally the low pulse flow wave. Similar results were found with pulse flow conditions at the frequency of 2 Hz (Li et al. 2009). To evaluate the level of hemodynamic energy, the energy equivalent pressure (EEP) was calculated according to the method described in a previous study (Undar et al. 2005). EEP was given by the formula: $EEP = (\int p f dt) / (\int f dt)$, where f was the flow rate, and p was the flow pressure. Pressure waves used to calculate hemodynamic energy were measured and shown in Fig. 5. The pressure and flow waveforms from the experimental measures showed similar wave contours, but there was a phase difference between them due to the pressure gradient in the flow area. As results, the EEP values for the high, medium and low pulse flow waves were 40, 24, and 8.3 mmHg, respectively. This analysis showed

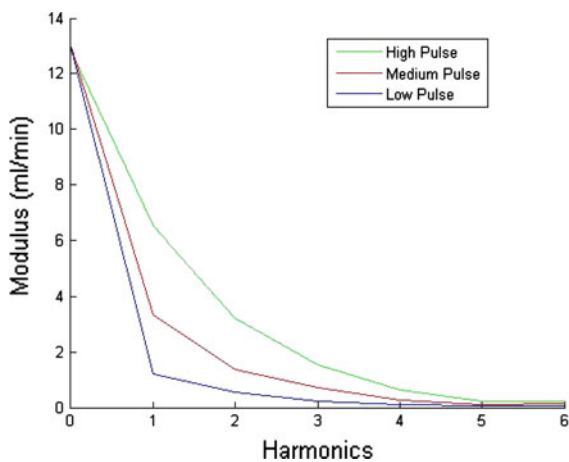


Fig. 4 Spectral analysis of the high, medium, and low pulse waveforms with harmonic modulus. The harmonic modulus shows the frequency component of the flow waveform for comparisons

that when the mean flow rate and the frequency were constant, a flow condition with a higher PI was characterized by a higher energy level. Therefore, the three quantitative descriptions of pulse flow waveforms yielded similar comparison results.

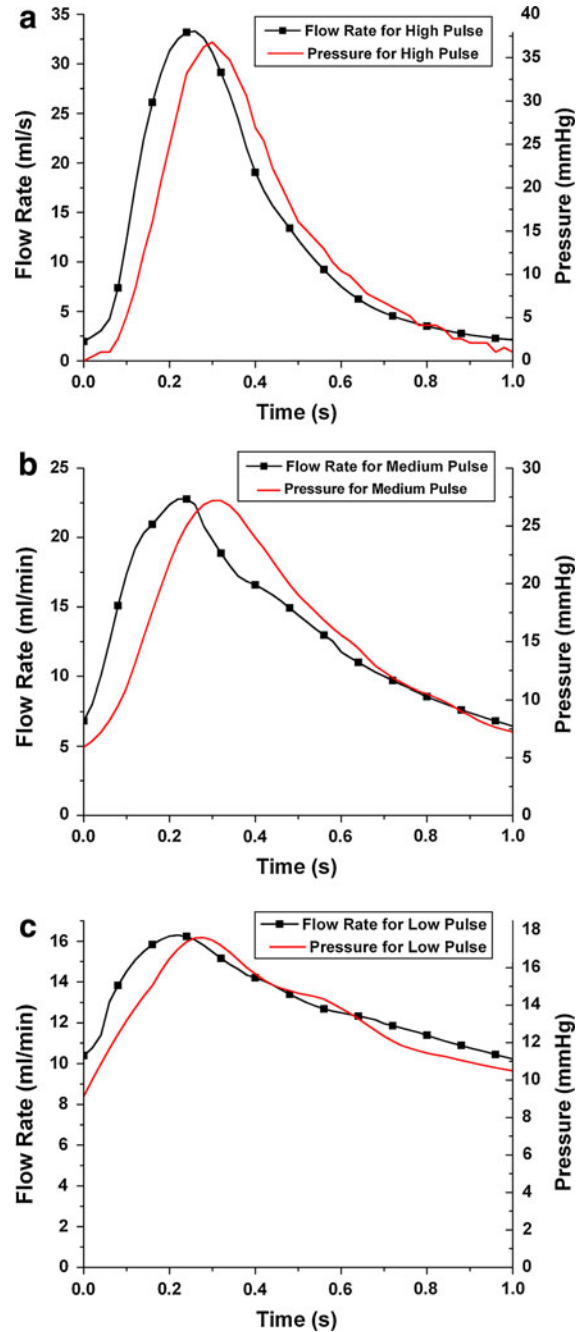


Fig. 5 Flow waves and pressure waves for the high (a), medium (b), and low (c) pulse flow conditions

Sensitivity analysis

In order to estimate the sensitivity of the inlet variables (i.e. mean flow rate and peak flow rate) to the outlet variable (i.e. shear stress) in the computational model, sensitivity analysis was performed according to the method described by Susilo et al. 2010. Cotter's method (Cotter 1979) the one-factor-at-a-time approach was used for this analysis. For each cycle, only one variable was changed to its upper or lower limit. For a model that takes the form of:

$$y = \Psi(\text{var}_1, \text{var}_2, \dots, \text{var}_n)$$

where y is the output, var_j is the variable and n is the number of variables, the number of cycles required is $2n + 2$. In order to determine the sensitivity for variable j , the following equation can be used (Susilo et al. 2010):

$$M(j) = \frac{1}{4} \left[\left(y_{2n+2} - y_{n+j+1} \right) + \left(y_{j+1} - y_1 \right) \right] + \frac{1}{4} \left[\left(y_{2n+2} - y_{n+j+1} \right) - \left(y_{j+1} - y_1 \right) \right]$$

Normalizing $M(j)$,

$$S_c(j) = \frac{M(j)}{\sum_1^n M(j)}$$

gives the sensitivity index, $S_c(j)$, for variable j .

Cell culture

Bovine PA ECs and SMCs were obtained from distal bovine vascular arteries from neonatal calves. Primary cells were used in the experiments because they retained most phenotypic characteristics and were more sensitive to environmental stimuli than immortal cell lines showing responses closer to cells responses in native tissue. These cells were maintained in Dulbecco's Modified Eagle's Medium (Cellgo DMEM, Mediatech Inc., Manassas/VA, USA), with 10% bovine calf serum (BCS) (Gemini Bio-products, West Sacramento/CA, USA) and 1% Pen/Strep (Invitrogen, Czarlsbad/CA, USA). Cell passages of 4–8 were used for all experiments. For flow experiments, the same medium condition was used. The entire flow system was placed in the incubator; CO_2 was supplied through the medium reservoir, as it allowed gas transfer to occur.

Flow co-culture of smooth muscle cells and endothelial cells

The EC-SMC co-culture was established under flow; SMCs were embedded in a collagen matrix and ECs were seeded on an isopore polycarbonate membrane with 0.8 μm pores (Millipore Corporate, Billerica/MA, USA). The collagen prepolymer solution was prepared by neutralizing type I collagen solution (BD Science, San Jose/CA, USA) with 7% NaHCO_3 and 0.1 M NaOH and increasing its ionic strength with PBS. A final collagen density of 2 mg/ml was obtained. The prepolymer solution was maintained on ice at a pH of 7.4, and SMCs (passage 3–6) detached from the culture flask were added to the solution with a density of 2×10^6 cells/ml. The cell/gel solution was mixed thoroughly, immediately transferred onto a functionalized glass slide, and spread to fully cover the surface.

Glass slides were chemically functionalized with aldehyde group which anchored the cell/gel under flow condition. The functionalization starts with introducing hydroxyl groups using 1 M NaOH. Then, amine groups formed on the slide surface via reaction with 95% of 3-aminopropyltriethoxysilane (Sigma Inc, St. Louis/MO, USA). Subsequently, an aldehyde crosslinker was added to the amine group via reaction with 1% (v/v) glutaraldehyde (Sigma Inc.) in phosphate buffer for 20 min. The yielded aldehyde forms linkage with primary amines on the macromolecular chains of collagen. The functionalized slide was immersed in 70% ethanol overnight. Collagen solution containing SMCs was pipetted into the gasket to fully cover the surface. The collagen-covered slides were then placed in an incubator for 30 min for gelation, which was followed by the addition of medium with 10% fetal bovine serum and cultured for 24 h.

For sterilizing the flow system, all the tubings were autoclaved. The flow chamber was made from acrylic and was sterilized in ethanol (70%) for 30 min prior to experiments, the porous membrane and the gaskets were autoclaved. To ensure sterility of the system, the pump and flow circulation without cultured cells were further sterilized with 30% hydrogen peroxide flowing throughout the circulation under UV light for 1 h, followed by flushing the system with sterile PBS.

To initiate co-culture, a porous membrane with a monolayer of EC was placed in contact with the SMC-collagen matrix. The monolayer of EC was established by seeding ECs with a density of 1×10^5 cells/ml

onto an autoclaved porous membrane. Cells were then grown till confluency.

To start flow study, a silicone gasket that fit around the periphery of the glass slide was placed on top of the EC-seeded membrane to subject ECs to the pulse flow waves. Two flow conditions, semi-steady flow (PI = 0.2) and medium pulse flow (PI = 1.68) with the same mean flow rate at a shear stress of 12 dyne/cm², were studied.

Real-time polymerase chain reaction

Total cellular RNA was extracted using RNeasy Mini Kit (Qiagen; Hilden, Germany) according to manufacturer's instructions. Complementary DNA was synthesized from 0.2 µg of total cellular RNA using iScript cDNA Synthesis Kit (Bio-Rad, Hercules/CA, USA). Real-time quantitative RT-PCR primers were designed using Primer 3 software, an open-source program widely-used for designing PCR primers (<http://primer3.sourceforge.net/>). The SYBR Green I assay and iCycler iQ real-time PCR detection system (Bio-Rad) were used to detect PCR products. The PCR thermal profile consisted of 95 °C for 10 min followed by 40 cycles of 95 °C for 15 s, 60 °C for 30 s and 95 °C for 1 min. Genes were normalized to the housekeeping gene hypoxanthine-guanine phosphoribosyl transferase (HPRT) and fold change relative to the static condition was calculated using the $\Delta\Delta CT$ method. The gene sequences are listed in Table 2.

Proliferating cell nuclear antigen assay

Proliferation was studied using immunochemical method of proliferating cell nuclear antigen (PCNA) (PCNA staining kit, Invitrogen, Carlsbad/VA, USA). The protocol on the product sheet was followed. Briefly, cells were fixed with acetone at -20 °C for 10 min. After fixation, cells were blocked for 10 min. Then, the primary antibody, a biotinylated PCNA monoclonal antibody (clone PC10), was applied to the slide for 1 h. This was followed by applying

streptavidin-peroxidase and dab chromogen for 10 and 5 min, respectively. The final step was to add hematoxylin for 2 min, followed by slide mounting. The cells were imaged with an upright light microscope. A brightly red stained nucleus indicated proliferating cells, whereas blue-stained nuclei showed non-proliferating cells. The percentage of proliferating cells out of total cells was determined.

Calculation of permeability

As the interstitial flow is important for sufficient amount of oxygen and nutrient concentration to the cells in a 3-D construct (Bjork 2009), the permeability of the collagen matrix that allows the interstitial flow to reach cells were determined. The hydraulic permeability of the 3-D SMC culture construct was determined from the equation of the permeability (K_p):

$$K_p = \frac{\mu(Q_i/A)}{(\Delta P/L)}$$

where μ is the fluid viscosity, Q_i is the volumetric flow rate to the interstitial flow, A is the cross sectional area of the gel and ΔP is the pressure drop over the length of the chamber (L).

Interstitial flow through the collagen was determined by the amount of flow that diffused into this matrix along the length of the chamber (Q_i). This is defined as $Q_i = Q_{in} - Q_{out}$. The average shear stress on the SMCs due to the interstitial flow can be expressed as:

$$\tau = \frac{\mu(Q_i/A)}{\sqrt{K_p}}$$

These values were calculated for high, medium and low pulse flow.

Statistical analysis

Statistical analysis was performed on the quantitative results of genetic analysis using a two-factor Analysis

Table 2 Primer sequences of bovine genes for real-time PCR analysis

Genes	Forward primer	Reverse primer
ICAM	GACTTCTTCAGCTCCCCAAG	CCCACATGCTATTTGTCCTG
MCP-1	CGDDTGCTGCTATACATTCA	ACACTTGCTGCTGGTGACTC
HPRT	CTGGCTCGAGATGTGATGAA	CAACAGGTCGGCAAAGAAGT

of Variance (ANOVA). A significance level of $P < 0.05$ was used. Four samples were used for each flow condition; statistical analysis was done to quantify the variation between these sample groups.

Results

Comparison of velocity profiles in different computational models

To explore the variations of flow profiles across the culture region, the centerline outlet velocities were used to compare three computational models (Fig. 6). Results showed that the velocity profiles along the length of the 2-D and 3-D rigid models were similar, which suggested that the 2-D model was an acceptable simplified representation of the 3-D model. Different from the two rigid models, the 2-D FSI model with a mimetic compliant structure resulted in more dampened flow waves at the outlet. Therefore, we used the 2-D FSI model to understand the propagation of pulse flow waves along the length of the chamber. The 3-D model was used to provide characterizations of flow across the width of the chamber, and to determine the entrance length and the wall effect length. The rigid model was suitable to produce these results because the non-rigid surface structure did not alter these values.

Spatial variation of pulse flow waves across the chamber width

To explore the effects of pulse flow waveform on cellular behaviors, it is important to identify a sampling region where all the selected cells are exposed to the same level of pulse flow (no significant differences in PI). Herein, this was achieved by examining spatial variations of temporal flow velocity profile. With the rigid 3-D model, we first characterized spatial variations of the flow velocity profiles along the length and across the width of the chamber at one time point. From this characterization, we determined the entrance length (the length from the inlet to the point where flow is fully developed) and the wall effect length (the length from the edge to the point where uniform flow is found). Results of the entrance

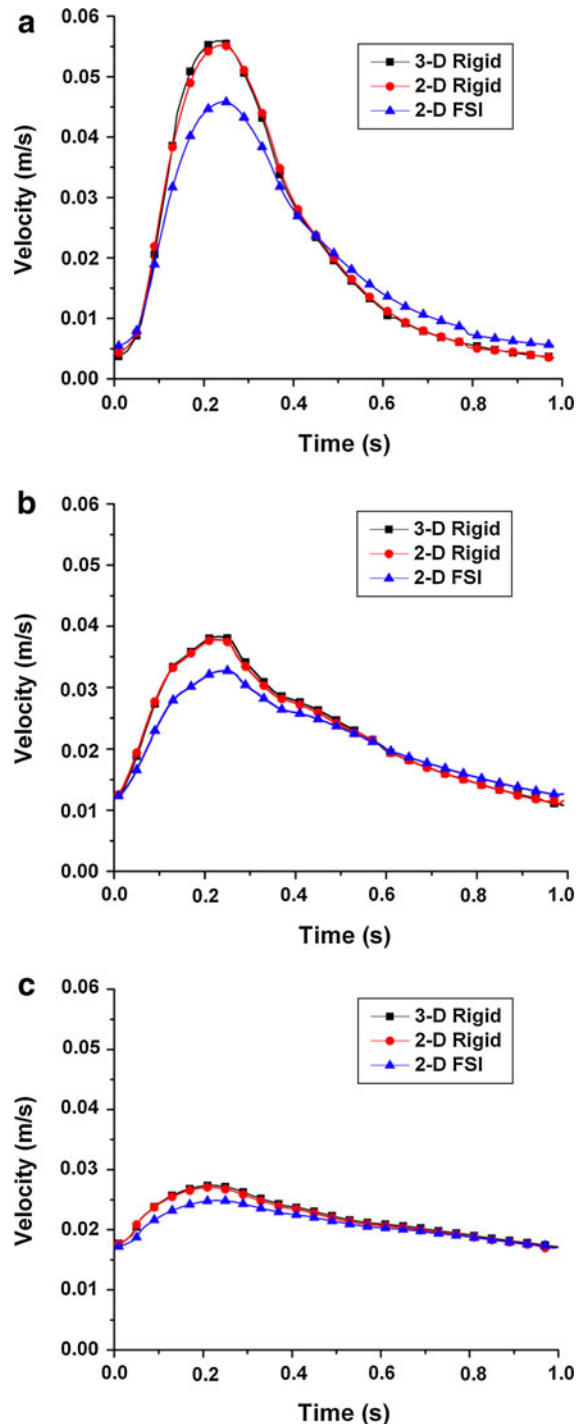


Fig. 6 Comparisons of velocity profiles generated by 3-D rigid, 2-D rigid, and 2-D FSI computational models. It is shown that the 3-D and 2-D rigid models result in similar waveforms for high (a), medium (b) and low (c) pulse waves

lengths for the three selected flow conditions (i.e. high, medium and low pulse flows) were shown in Table 3. The corresponding velocity color map is shown in Fig. 7, where the region of uniform velocity is outlined, the velocity at the walls and the entrance changed (shown by a color change from the middle of the chamber). No significant differences in the entrance length were found among the three flow conditions; all the entrance lengths were around 4×10^{-4} m (or 0.4 mm). Results of the wall effect lengths are shown in Table 3. The corresponding velocity color map is shown in Fig. 7. The wall effect length illustrated the effect of friction due to the sidewalls which reduced the motion of the fluid. No significant differences in the wall effect length were found among the three flow conditions; the lengths for all pulse flow conditions were around 0.027 mm. Our results also showed that the entrance length and the wall effect length were nearly constant over time. The velocity color map showed slower velocities at the edges and at the entrance (or exit), and a uniform velocity across the rest of the width and length. Therefore, a uniform temporal velocity profile was present in the majority of the chamber. In addition to the entrance length region and wall effect region, disturbed flow was also found at the corners of the chamber, but this did not affect the overall flow field

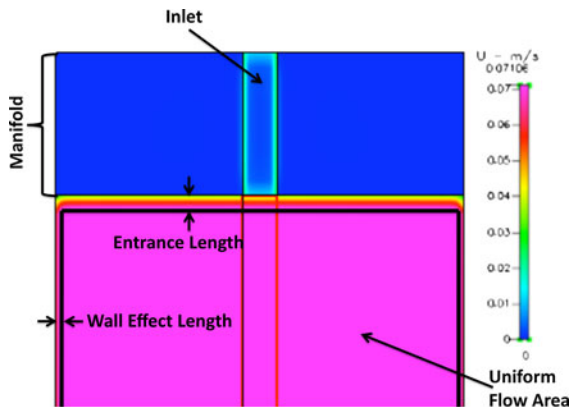


Fig. 7 The velocity color map (output from the 2-D FSI model) shows the velocity change throughout the channel and shows the entrance length to uniform velocity and the effects of the sidewalls and the uniform flow area. The uniform velocity region is outlined. In this region, the pulse flow velocity is constant over the time, represented by the same color throughout. A color change at the side walls and at the entrance of the chamber indicates that the pulse flow velocity decreases in those regions which are not included in the identified region for cell analysis. (Color figure online)

and was not included in the region for cell sampling (supporting information: S-Figure 1).

The flow shear stress in the chamber was calculated based on the spatial derivative of velocity. Table 4 shows the averages of peak and mean shear stresses for the three flow waves in the identified uniform flow region.

Although the fluid layer directly adjacent to the cells was used for the flow profiles in this study, the spatial velocity over the depth was examined to fully understand spatial flow profiles. The boundary layer can be developed in the thickness direction. Results showed that a fully developed parabolic flow was present in the thickness direction (supporting information: S-Figure 2), different from the underdeveloped flow (flat flow profile) across the width of the chamber.

Wave propagation of pulse flows

Flow wave propagations along the length of the chamber were examined using the 2-D FSI model. This model resulted in more accurate flow propagation profiles due to the inclusion of the parameters of membrane and gel. To study the propagation of the flow profile along the length of the chamber, a flow waveform was obtained from the computational model at different longitudinal points along the

Table 3 The computational model determined the entrance length and the wall effect length

Velocity wave	Entrance length (mm)	Wall effect length (mm)
Low pulse	0.46	0.027
Medium pulse	0.45	0.027
High pulse	0.46	0.027

The entrance length was measured from the exit of the reservoir to the point of uniform velocity along the centerline of the chamber. The wall effect length was measured from the sidewall to the point of uniform velocity

Table 4 Mean and peak shear stresses for the low, medium and high pulse flow waves

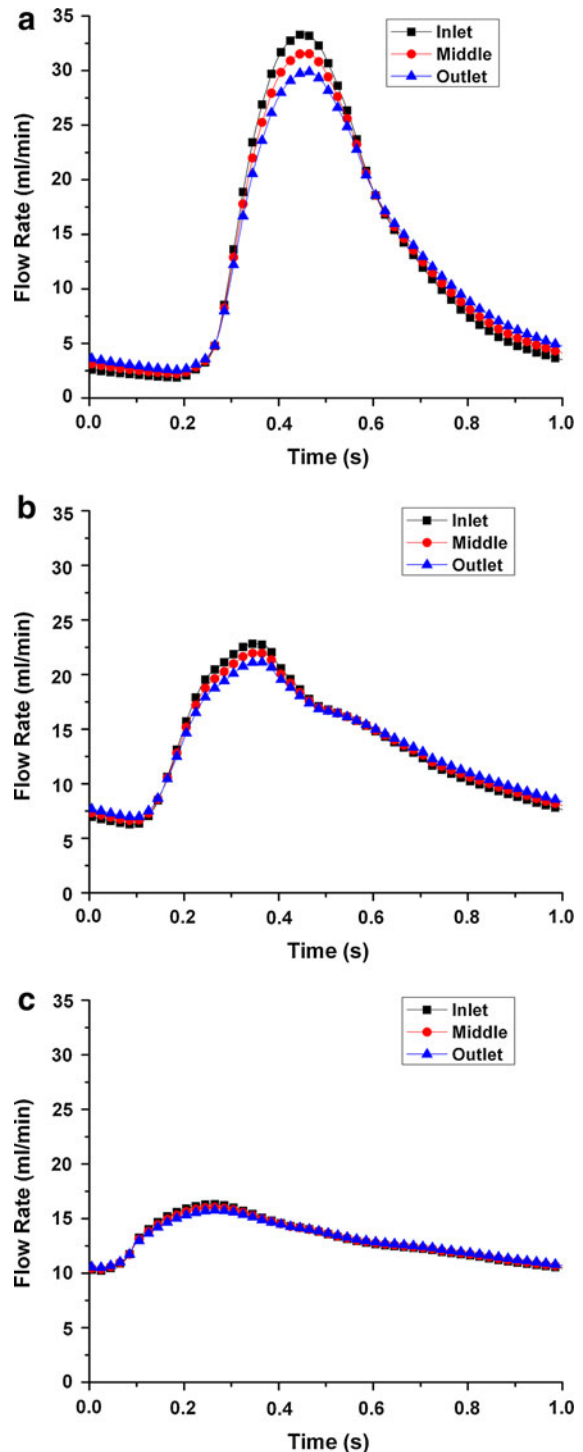
Velocity wave	Mean shear (dyne/cm ²)	Peak shear (dyne/cm ²)
Low pulse	12.19	15.13
Medium pulse	12.51	20.06
High pulse	11.91	30.04

Fig. 8 Spatial variations of flow waves. Flow time-history waves for the three pulse flow conditions, high (a), medium (b), low (c), were tested in three regions of the chamber, near the inlet, in the middle of the channel, and near the exit of the 2-D compliant model. These flow waves indicate that pulse flow is not changing in the identified region

chamber, i.e. near the inlet, in the middle and near the outlet of the chamber for each of the three selected flow conditions. All the selected points were located in the identified uniform flow region in Sect. “Spatial variation of pulse flow waves across the chamber width”. Results showed that flow waveform slightly varied in that region, evident in the fact that there was a small decrease in flow time-histories along the length of the channel as the wave propagated (Fig. 8). This could be attributed to a small amount of energy was dissipated as the flow waves traveled through the culture channel; the substrate was slightly deformable impeding the wave propagation. Whereas in the rigid 2-D and 3-D models, the propagation of flow waves through the entire flow region was instantaneous due to the lack of deformability. The 2-D FSI model gave a more accurate demonstration of flow behaviors down the length of the chamber. As the flow propagated to the middle and outlet, the FSI model resulted in slightly dampened flow. However, the dampening effect was not significant, and therefore the identified uniform region was still considered effective, which was validated and affirmed with cellular assays.

Comparison of experimental measures with computational model results

A comparison of the velocity profiles from experimental measures with those from the 2-D FSI computational model provided a validation of the test section function. The comparisons between 2-D FSI model and experimental measure were made with outlet velocities for the high, medium and low pulse flow waves (Fig. 9). The largest percent difference between the computational and experimental outlet velocities was found to be <10%, which occurred in the case of high pulse flow wave. A corrected waveform for high pulse flow was developed for the comparison due to some limitations in that experimental setup. The other flow waves showed a smaller amount of discrepancy, <5% for the medium pulse flow and <1% for the low pulse flow. These differences were small enough to be considered as



acceptable discrepancies. These result showed that the velocities along the experimental chamber and the calculated shear stresses were very close to the actual shear stresses.

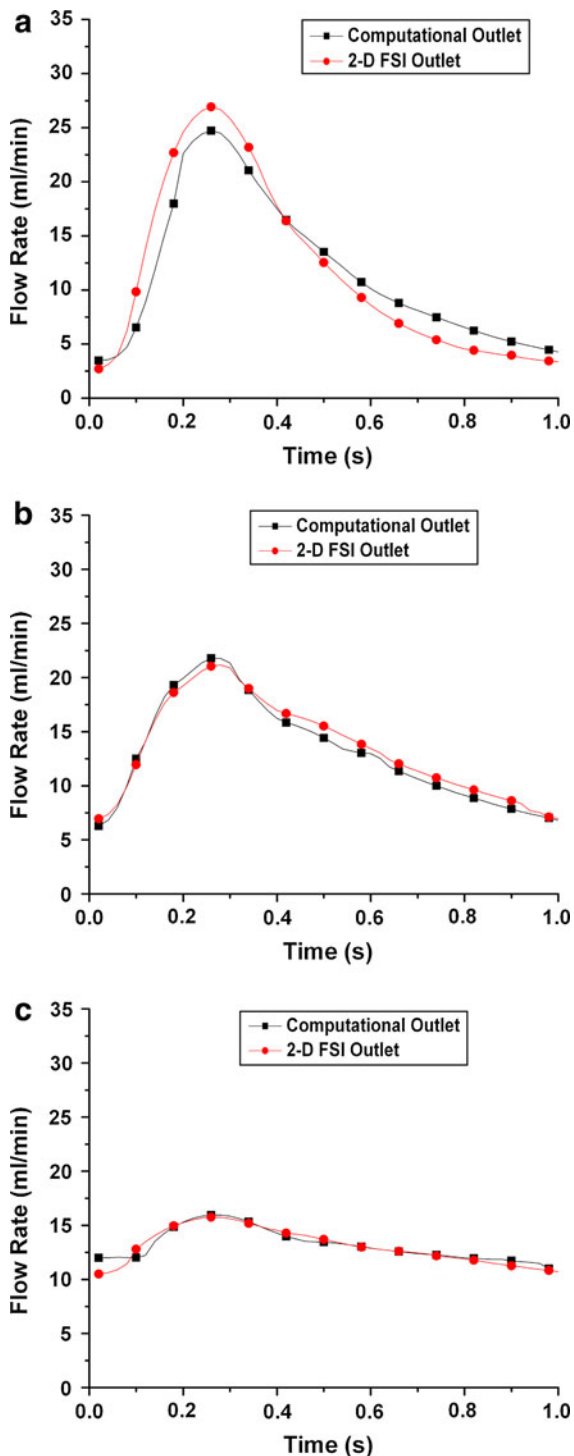


Fig. 9 Comparisons of the outlet velocity waves between the computation and experiment results for high (a), medium (b) and low (c) pulse flow conditions. This verifies the computation model, showing a small but expectable <10% deviation between experiment and computation

Sensitivity analysis

Sensitivity analysis was performed on the mean and peak inlet flow rates to determine their effects on the model. Average outlet shear stress was used as the output for Cotter's method. The upper and lower limits for this method were 10% increase or decrease in the variables. The sensitivity index, S_c , for the mean flow rate was 0.41, while that for the peak flow rate was 0.59. The results indicated that the model was slightly more sensitive to peak flow rate.

Validation using endothelial gene expression

In addition to comparison of experimental flow measurements with computational simulations, we have evaluated cell responses to the pulse flow condition vs semi-steady flow condition to verify the identified uniform flow region. The EC pro-inflammatory gene expression and SMC proliferation in response to flow provided a validation of the test section with respect to molecular signaling. Previous studies have demonstrated the ability of ECs to discriminate among flow patterns (Dai et al. 2004; Davies 2009; Chien 2007; Gimbrone et al. 2006; Reneman et al. 2006). They also showed that there existed a narrow homeostatic range of stresses in the vascular system; small perturbation of hemodynamic stress levels led to the activation of inflammation events in the endothelium and ultimately proliferation of SMCs (Walshe et al. 2005; Hastings et al. 2007). Thus, genetic analysis of endothelial responses to flow in the chamber represents a biological validation of computational design.

ECs were sampled from different regions in the uniform shear stress area, and real-time PCR method was used to compare EC gene expression of pro-inflammatory molecules. The mRNA expressions of ICAM-1 and MCP-1 in ECs were known to be highly responsive to the small changes in flow conditions (Shyy et al. 1994; Hsiai et al. 2003; Tsubio et al. 2006; Yee et al. 2008). In agreement with these studies, we found that a significant difference existed between the mRNA expression of ICAM-1 and MCP-1 for the semi-steady flow condition (control) and the medium pulse flow condition (experiment) (Fig. 10). However, there were no statistically significant differences in EC expressions of ICAM-1 mRNA and MCP-1 mRNA

among the different sampling regions (near the inlet, in the middle and near the outlet). This result further affirmed that the slight differences in temporal pulse flow profiles along the chamber length were still within the range that induced uniform cell expression.

Validation using SMC proliferation in the developed co-culture device

Endothelial cells on the blood vessel wall act as mechanical sensors to transduce mechanical signals into biochemical signals that modulate the activities of other cells such as SMC (Hahn and Schwartz 2009). Therefore, SMC proliferation was used as another biological validation of the sampling region with respect to mechanotransduction and molecular signaling.

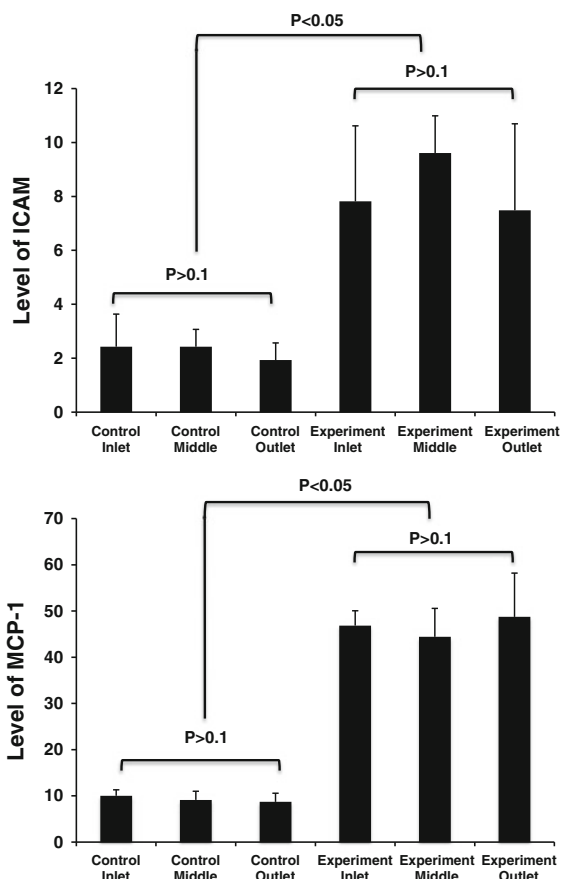


Fig. 10 ICAM-1 and MCP-1 mRNA expressions in ECs subjected to flow. Polymerase chain reaction results demonstrate that ECs in the CFD-identified uniform region showed similar ICAM-1 and MCP-1 mRNA expressions. Also, there is a significant difference in these expressions between semi-steady flow (control) and pulse flow (experiment)

Results showed that no statistically significant difference existed for SMC proliferations at the inlet, middle and outlet of the chamber for each condition (Fig. 11), while medium pulse flow increased SMC proliferation when compared to semi-steady flow. Endothelial protection of SMCs was thus demonstrated for semi-steady flow condition which small vascular cells experience in physiological conditions. With increased flow pulsatility, small vascular EC on a stiff substrate tended to lose this protective function. Here SMCs were grown in serum-containing medium, and thus the cells were not arrested in a quiescent state prior to the determination of cell proliferation. Cells yielded higher proliferation (~30–40% of cells showing PCNA) than those pre-arrested in the quiescent state (less than 10% of cells showing PCNA).

In order to ensure the transport of oxygen and nutrient was sufficient for cell survival and metabolism, the permeability of medium through the construct was determined. Results showed that the permeability values of the porous membrane and collagen for low, medium and high pulse flow were $1.02 \times 10^{-7} \text{ cm}^2$, $7.17 \times 10^{-7} \text{ cm}^2$, $1.91 \times 10^{-6} \text{ cm}^2$, respectively. The interstitial flows for low, medium and high pulse flows were $6.32 \times 10^{-3} \text{ ml/min}$, $4.56 \times 10^{-2} \text{ ml/min}$ and $11.38 \times 10^{-2} \text{ ml/min}$, respectively. The interstitial flow is an important determinant to the availability of oxygen and nutrients to SMCs. With the porous membrane and 3-D matrix design, we have shown that

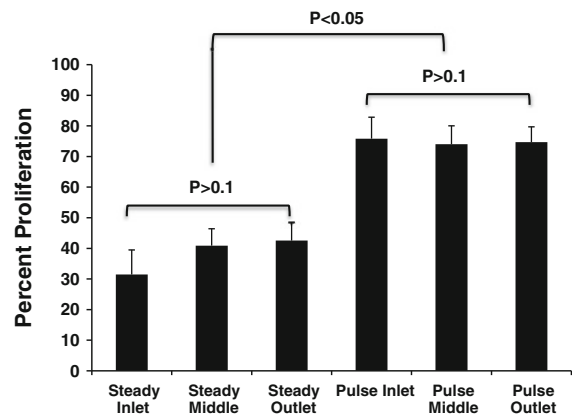


Fig. 11 SMC PCNA expression under flow. Results on PCNA expressions by SMC demonstrate that cells in the CFD-identified uniform region showed similar proliferation in 10% serum medium. But there is a significant difference in SMC proliferation between the co-culture under semi-steady flow and that under pulse flow

the interstitial flow is >0.0063 ml/min (or >9 ml/day), which allows sufficient diffusion of nutrients and oxygen to enable SMC survival and metabolism. In addition, normal transmural interstitial flows can expose SMCs to shear stresses; though they are much lower than those ECs are exposed to, strong interstitial flow-derived shear stress around the SMC may cause shear-induced cell necrosis (Chung et al. 2007). Based on the interstitial flow, we determined the shear stresses around the SMC for low, medium and high pulse flows were 0.0015, 0.013, 0.06 dyne/cm², respectively. Thus, the interstitial flows around SMCs found here were not high enough to cause cell necrosis when compared with other studies (Bjork 2009). Further studies may need to be conducted on this subject to quantify the distribution of oxygen and nutrients throughout the collagen matrix.

Both Figs. 10 and 11 are experimental validations of the computational study results, demonstrating uniform flow dynamics in the chamber from the cells' perspective, which reflects the design goal. Figure 10 shows response of ECs with PCR for the expression of ICAM-1 and MCP-1, two flow-sensitive pro-inflammatory genes, confirming the computational results for uniform EC response to flow in the designated uniform area. Figure 11 further shows uniform SMC responses in the identified area.

Discussion

The present study has developed a flow co-culture system, in which arterial-like pulse flows with varied pulsatility were imposed on EC-SMC co-culture, mimic the vessel wall. The new system thus connects upstream stiffness to downstream vascular cell co-cultures through pulse flow dynamics. The novelty of this system lies in the inherent connection between this flow co-culture system and the stiffness-induced vascular cell remodeling in the circulation. The flow variations in the co-culture chamber have been characterized with CFD model and validated with experimental measures and cell assays. The structurally-based CFD model was developed to account for the spatial variation and wave propagation of pulse flow waves as well as variations in temporal profiles of velocities and shear stresses in the flow chamber; the results guide the design of the chamber and identify sampling regions for cell assays. Flow measurements

and cell analyses further validated the identified uniform flow region. Cells from that region thus could be used to explore the effects of pulse flow wave (flow pulsatility) on vascular cell remodeling. Results showed that the flow culture chamber was characterized by a large area of uniform flow, a feature important for studies of cell signaling such as protein phosphorylation assay needing a large number ($>10^5$) of cells. Collectively, the present study provided a new and simple system for investigating the mechanistic relationship between arterial stiffening, flow pulsatility and vascular remodeling. As vascular stiffening is an emerging topic in the area of arterial diseases, the new system may find broad applications.

There are several unique aspects in this study. First, this study compared computational results with both experimental flow measurements and cell analyses including gene and protein analyses. As demonstrated by the comparison between the computational and experimental outlet flow waves, the computed flow profiles were very close to the experimental profiles. Verification with biomolecular analysis, from the cells' perspective, provided unique biological evidence that CFD design parameters accurately described the pulse flow behaviors in the flow chamber. The pro-inflammatory markers were chosen due to their sensitivity to flow shear and their relevance to pulmonary hypertension. Second, the new system accommodates a co-culture of cells with a biomimetic arrangement, in which EC is under the influence of pulsatile flow shear stress, SMC are in the 3-D collagen matrix, and EC/SMC communicate through 0.8 μ m pores that simulate the function of fenestral pores ranging from 0.4 to 2.1 μ m in diameter (Tada and Tarbell 2000). Compared to previous studies which investigated EC/SMC co-cultures under static or steady flow conditions (Fillinger et al. 1997; Chiu et al. 2003; Heydarkhan-Hagvall et al. 2003), this flow system allows one to explore vascular remodeling under biomimetic flow and culture environments. Third, the unique flow system developed here conveniently generates a series of pulse flow waves that simulate diastolic and systolic phases of arterial flow. More importantly, changes in diastolic and systolic phases of these pulse flow waveforms correlate with changes in flow pulsatility and upstream stiffness while maintaining the same mean flow rate. This allows separation of flow pulsatility effects (i.e. temporal variation of flow) from flow magnitude effects. This

separation represents a major departure from most previous flow mechanobiology studies which often employ reduced and/or oscillatory flow conditions (Davies 2009; Chien 2007). As it has become increasingly known that the analysis of pulse wave contour in relation to arterial stiffness has the potential to determine risk for cardiovascular diseases, pulse flow waveform or flow pulsatility was quantitatively described with several methods in the present study. The system presented here also allows a variety of signaling mechanism studies due to the capability of sampling a large number of cells under a statistically homogeneous high-fidelity pulse flow wave. Therefore, the developed flow system may be useful to explore cell mechanobiology mechanism in response to pulse flow variations such as those due to arterial stiffening.

The system presented here to regulate flow pulsatility is unique and different from a recent study which used a pneumatic pump to program air pressure changes for the production of pulsatile flow (Shi 2008). It is an important feature to simulate vascular system *in vivo* with the same mean flow rate and flow pressure. The pulse pressure adjustment function was achieved by changing the volume of air in the upstream stiffness-adjustment chamber. As air is compressible, it can absorb the pressure energy of high pulse flow decreasing the flow PI, while discharging the pressure energy to increase the flow when the pressure is low. As a result, air in the chamber stiffness-adjustment dampened the flow pulsatility; the more air in the chamber, the lower level of flow pulsatility.

Results from this study may be applied to a range of chamber designs and flow conditions, yielding a large uniform flow region for cell studies. For pulse flow conditions, the spatial velocity profile is affected by the womersley number that expresses pulse frequency in relation to viscous effects. An alternative method to produce a larger uniform region is to reduce the channel height, which can decrease the womersley number yielding similar results as increasing the frequency, according to the womersley number definition. In the present study, a frequency of 1 Hz yields a womersley number of 1.44. At this womersley number, a flat, blunt flow profile pervades the chamber. This is in good agreement with previous studies (Nauman et al. 1999; Chung et al. 2003).

Several limitations need to be acknowledged. The computational model is a simplistic representation of

the experimental flow chamber; as a result, the computational model does not identically replicate the experimental flow chamber (<10% error). CFD was used solely as a design tool to define a uniform region of pulsatile flow and to give a close estimate of the velocities and shear stresses that cells experience. Another limitation occurs in the experimental measurement. The accuracy of experimental measurements with a flow meter is dependent on the speed of the computer communication. The optimal refreshing rate of flow velocity measurements in this study is 10 ms. Thus, the communication speed may not be fast enough to provide accurate measurement if the flow rate changes within 10 ms. Given that most human flow conditions do not contain significant energy content beyond 10 Hz, this limitation should not have a significant impact.

Conclusion

This study has developed and characterized a new flow system that exposes co-cultured cells to arterial-like pulse flow waves. CFD models as well as experimental measurements and biomolecular analyses together were used to define a uniform flow region for cell mechanobiology studies. This flow system enables one to study the effects of upstream stiffness and pulse flow energy on EC and SMC. This system thus provides a valuable tool to study vascular cell remodeling in relation to mechanical environment involving changes in vascular stiffness or flow pulsatility.

Acknowledgments The authors wish to thank CVP group for providing the cells and acknowledge funding from American Heart Association (SDG 2110049 to W.T.), and NIH (HL K25 097246 to W.T., HL T32 072738 to R.S.).

References

- Berger RMF, Cromme-Dijkhuis AH, Hop CJ, Kruit MN, Hess J (2002) Pulmonary arterial wall distensibility assessed by intravascular ultrasound in children with “congenital heart disease an indicator for pulmonary vascular disease?”. *Chest* 122:549–557
- Bjork TR (2009) Transmural flow bioreactor for vascular tissue engineering. *Biotechnol Bioeng* 104:1197–1206
- Chesler NC, Thompson-Figueroa J, Millburne K (2004) Measurements of mouse pulmonary artery biomechanics. *J Biomech Eng* 126:309–314
- Cheung N, Sharrett AR, Klein R, Criqui MH, Islam FM, Macura KJ, Cotch MF, Klein BE, Wong TY (2007) Aortic

- distensibility and retinal arteriolar narrowing: the multi-ethnic study of atherosclerosis. *Hypertension* 50:617–622
- Chien S (2007) Mechanotransduction and endothelial cell homeostasis: the wisdom of the cell. *Am J Physiol Heart Circ Physiol* 292:H1209–H1224
- Chiu JJ, Chen LJ, Lee PL, Lee CI, Lo LW, Usami S, Chien S (2003) Shear stress inhibits adhesion molecule expression in vascular endothelial cells induced by coculture with smooth muscle cells. *Blood* 101:2667–2674
- Chung BJ, Roberston AM, Peters DG (2003) The numerical design of a parallel plate flow chamber for investigation of endothelial cell response to shear stress. *Comput Struct* 81:535–546
- Chung CC, Chen CP, Tseng CS (2007) Enhancement of cell growth in tissue-engineering constructs under direct perfusion: modeling and simulation. *Biotechnol Bioeng* 97:1603–1616
- Cotter S (1979) A screening design for factorial experiments with interactions. *Biometrika* 66:317–320
- Dai G, Kaazempur-Mofrad MR, Natarajan S, Zhang Y, Vaughn S, Blackman BR, Kamm RD, Garcia-Cardena G, Gimbrone MA (2004) Distinct endothelial phenotypes evoked by arterial waveforms derived from atherosclerosis-susceptible and resistant regions of human vasculature. *Proc. Natl. Acad. Sci. USA* 101:14871–14876
- Davies PF (2009) Hemodynamic shear stress and the endothelium in cardiovascular pathophysiology. *Nat Clin Pract Cardiovasc Med* 6:16–26
- Fillinger MF, Sampson LN, Cornenwett JL, Powell RJ, Wagner RJ (1997) Coculture of endothelial cells and smooth muscle cells in bilayer and conditioned media models. *J Surg Res* 67:169–178
- Gimbrone MA, Topper JN, Nagel T, Anderson KR, Garcia-Cardena G (2006) Endothelial dysfunction, hemodynamic forces, and atherogenesis. *Ann NY Acad Sci* 902:230–240
- Gorgulu S, Eren M, Yildirim A, Ozer O, Uslu N, Celik S, Dagdeviren B, Nurkalem Z, Bagirtan B, Tezel T (2003) A new echocardiographic approach in assessing pulmonary vascular bed in patients with congenital heart disease: pulmonary artery stiffness. *Anadolu Kardiyol Derg* 3: 92–97
- Hahn C, Schwartz MA (2009) Mechanotransduction in vascular physiology and atherogenesis. *Nat Rev Mol Cell Biol* 10:53–62
- Hastings NE, Simmers MB, McDonald OG, Wamhoff BR, Blackman BR (2007) Atherosclerosis-prone hemodynamics differentially regulates endothelial and smooth muscle cell phenotypes and promotes proinflammatory priming. *Am J Physiol Cell Physiol* 293:1824–1833
- Heydarkhan-Hagvall S, Helenius G, Johanasson BR, Li JY, Mattsson E, Risberg B (2003) Co-culture of endothelial cells and smooth muscle cells affect gene expression of angiogenic factors. *J Cell Biochem* 89:1250–1259
- Hsiai TK, Cho SK, Honda HM, Hama S, Navab M, Demer LL, Ho CM (2002) Endothelial cell dynamics under pulsating flows: significance of high versus low shear stress slew rates. *Ann Biomed Eng* 30:646–656
- Hsiai TK, Cho SK, Wong PK, Ing M, Salazar A, Sevanian A, Navab M, Demer LL, Ho CM (2003) Monocyte recruitment to endothelial cells in response to oscillatory shear stress. *FASEB J* 17:1648–1657
- Hunter K, Lee P, Lanning C, Ivy D, Kirby K, Claussen L, Chan K, Shandas R (2008) Pulmonary vascular input impedance is a combined measure of pulmonary vascular resistance and stiffness and predicts clinical outcomes better than pulmonary vascular resistance alone in pediatric patients with pulmonary hypertension. *Am Heart J* 155:166–174
- Li M, Scott D, Shandas R, Stenmark KR, Tan W (2009) High pulsatility flow induces adhesion molecule and cytokine mRNA Expression in distal pulmonary artery endothelial cells. *Ann Biomed Eng* 37:1082–1092
- McVeigh GE, Bratteli CW, Morgan DJ, Alinder CM, Glasser SP, Finkelstein SM, Cohn JN (1999) Age-related abnormalities in arterial compliance identified by pressure pulse contour analysis. *Hypertension* 33:1392–1398
- Mitchell GF (2008) Effects of central arterial aging on the structure and function of the peripheral vasculature: implications for end-organ damage. *J Appl Physiol* 105: 1652–1660
- Nauman EA, Ristic KJ, Keaveny TM, Satcher RL (1999) Quantitative assessment of steady and pulsatile flow fields in parallel plate flow chamber. *Ann Biomed Eng* 27:194–199
- O'Rourke MF, Safar ME (2005) Relationship between aortic stiffening and microvascular disease in brain and kidney: cause and logic of therapy. *Hypertension* 46:200–204
- Panaritis V, Kyriakidis AV, Pyrgioti M, Raffo L, Anagnostopoulou E, Gourniezaki G, Koukou E (2005) Pulsatility index of temporal and renal arteries as an early finding of arteriopathy in diabetic patients. *Ann Vas Sur* 19:80–83
- Reneman RS, Arts T, Hoeks APG (2006) Wall shear stress—an important determinant of endothelial cell function and structure—in the arterial system in vivo. *J Vasc Res* 43: 251–269
- Safar ME, Lacolley P (2007) Disturbance of macro- and micro-circulations: relations with pulse pressure and cardiac organ damage. *Am J Physiol Heart Circ Physiol* 293: H1–H7
- Safar ME, Levy BI, Struijker-Boudier H (2003) Current perspectives on arterial stiffness and pulse pressure in hypertension and cardiovascular diseases. *Circulation* 107:2864–2869
- Sakao S, Tatsumi K, Voelkel NF (2009) Endothelial cells and pulmonary arterial hypertension: apoptosis, proliferation, interaction and transdifferentiation. *Respir Res* 10:95
- Shi Y (2008) Numerical simulation of global hydro-dynamics in a pulsatile bioreactor for cardiovascular tissue engineering. *J Biomech* 41:953–959
- Shyy YJ, Hsieh HJ, Usami S, Chien S (1994) Fluid shear stress induces a biphasic response of human monocyte chemotactic protein 1 gene expression in vascular endothelium. *Proc. Natl. Acad. Sci. USA* 91:4678–4682
- Susilo M, Roeder BA, Voytik-Harbin SL, Lokini K, Nauman EA (2010) Development of a three dimensional unit cell to model the micromechanical response of a collagen-based extracellular matrix. *Acta Biomater* 6:1471–1486
- Tada A, Tarbell JM (2000) Interstitial flow through the internal elastic lamina affects shear stress on arterial smooth muscle cells. *Am J Physiol Heart Circ Physiol* 278:H1589–H1597
- Tsubio H, Ando J, Korenaga R, Takada Y, Kamiya A (2006) Flow stimulates ICAM-1 expression time and shear stress dependently in cultured human endothelial cells. *Biochem Biophys Res Comm* 6:988–996

- Undar A, Zapanta CM, Reibson JD, Souba M, Lukic B, Weiss WJ, Snyder AJ, Kunselman AR, Peirce WS, Rosenberg G, Myers JL (2005) Precise quantification of pressure flow waveforms of a pulsatile ventricular assist device. *ASAIO* 51:56–59
- Walshe TE, Ferguson G, Connell P, O'Brien C, Cahill PA (2005) Pulsatile flow increases the expression of eNOS, ET-1, and prostacyclin in a novel in vitro coculture model of the retinal vasculature. *Invest Ophthalmol Vis Sci* 46:375–382
- Weber T, Auer J, O'Rourke MF, Kvas E, Lassnig E, Berent R, Eber B (2004) Arterial stiffness, wave reflections, and the risk of coronary artery disease. *Circulation* 109:184–189
- Yee A, Bosworth KA, Conway DE, Eskin SG, McIntire LV (2008) Gene expression of endothelial cells under pulsatile non-reversing vs. steady shear stress; comparison of nitric oxide production. *Ann Biomed Eng* 36:571–579